

ARMY RESEARCH LABORATORY



**Computational Fluid Dynamics Flow Field Solutions for a
Kinetic Energy (KE) Projectile With Sabot**

by Karen R. Heavey, James DeSpirito, and Jubaraj Sahu

ARL-MR-572

September 2003

NOTICES

Disclaimers

The findings in this report are not to be construed as an official Department of the Army position unless so designated by other authorized documents.

Citation of manufacturer's or trade names does not constitute an official endorsement or approval of the use thereof.

Destroy this report when it is no longer needed. Do not return it to the originator.

Army Research Laboratory

Aberdeen Proving Ground, MD 21005-5066

ARL-MR-572

September 2003

Computational Fluid Dynamics Flow Field Solutions for a Kinetic Energy (KE) Projectile With Sabot

**Karen R. Heavey, James DeSpirito, and Jubaraj Sahu
Weapons and Materials Research Directorate, ARL**

Report Documentation Page			<i>Form Approved</i> <i>OMB No. 0704-0188</i>	
Public reporting burden for this collection of information is estimated to average 1 hour per response, including the time for reviewing instructions, searching existing data sources, gathering and maintaining the data needed, and completing and reviewing the collection information. Send comments regarding this burden estimate or any other aspect of this collection of information, including suggestions for reducing the burden, to Department of Defense, Washington Headquarters Services, Directorate for Information Operations and Reports (0704-0188), 1215 Jefferson Davis Highway, Suite 1204, Arlington, VA 22202-4302. Respondents should be aware that notwithstanding any other provision of law, no person shall be subject to any penalty for failing to comply with a collection of information if it does not display a currently valid OMB control number. PLEASE DO NOT RETURN YOUR FORM TO THE ABOVE ADDRESS.				
1. REPORT DATE (DD-MM-YYYY) September 2003		2. REPORT TYPE Final		3. DATES COVERED (From - To) January 2002 – May 2003
4. TITLE AND SUBTITLE Computational Fluid Dynamics Flow Field Solutions for a Kinetic Energy (KE) Projectile With Sabot			5a. CONTRACT NUMBER	
			5b. GRANT NUMBER	
			5c. PROGRAM ELEMENT NUMBER	
6. AUTHOR(S) Karen R. Heavey, James DeSpirito, and Jubaraj Sahu			5d. PROJECT NUMBER 1L162618AH80	
			5e. TASK NUMBER	
			5f. WORK UNIT NUMBER	
7. PERFORMING ORGANIZATION NAME(S) AND ADDRESS(ES) U.S. Army Research Laboratory ATTN: AMSRL-WM-BC Aberdeen Proving Ground, MD 21005-5066			8. PERFORMING ORGANIZATION REPORT NUMBER ARL-MR-572	
9. SPONSORING/MONITORING AGENCY NAME(S) AND ADDRESS(ES)			10. SPONSOR/MONITOR'S ACRONYM(S)	
			11. SPONSOR/MONITOR'S REPORT NUMBER(S)	
12. DISTRIBUTION/AVAILABILITY STATEMENT Approved for public release; distribution is unlimited.				
13. SUPPLEMENTARY NOTES				
14. ABSTRACT A study was undertaken to investigate and analyze the flow field results produced by various computational solvers for a projectile of interest to the U.S. Army. Computational fluid dynamics (CFD) techniques were used to obtain numerical solutions for the flow field of a kinetic energy projectile with the original and a modified (experimental) sabot. Computed results were obtained at Mach 4.5 and a 0° angle of attack. Qualitative flow field features showed the pressure on the surface of the model as well as pressures in the flow field. The surface pressure data on the projectile were extracted from the solution files and compared. In all cases, the results were comparable. These results show the predictive capabilities of CFD techniques in the analysis of supersonic flow over projectiles with sabots. They also provide an insight into the software capabilities of several of the many tools available to research scientists in the field of CFD.				
15. SUBJECT TERMS computational fluid dynamics (CFD), projectile aerodynamics, projectile with sabot, structured and unstructured grids				
16. SECURITY CLASSIFICATION OF:			17. LIMITATION OF ABSTRACT UL	18. NUMBER OF PAGES 30
a. REPORT UNCLASSIFIED	b. ABSTRACT UNCLASSIFIED	c. THIS PAGE UNCLASSIFIED		
			19b. TELEPHONE NUMBER (Include area code) 410-278-2916	

Contents

List of Figures	iv
List of Tables	v
Acknowledgments	vi
1. Introduction	1
2. Flow Solvers	1
2.1 ZNSFLOW Code.....	1
2.2 CFD++ Code	2
2.3 FLUENT Code	3
3. Projectile and Model Geometry	4
3.1 Projectile System.....	4
3.2 Computational Models	4
4. Computational Meshes	5
4.1 ZNSFLOW Grids	5
4.2 CFD++ Grids.....	6
4.3 FLUENT Grids.....	7
5. Results	8
5.1 Original Sabot.....	8
5.2 Modified Sabot	12
5.3 Force Comparison	16
5.4 Solver Differences.....	19
6. Conclusion	20
7. References	21

List of Figures

Figure 1. Drawing of an M829A2 round.	4
Figure 2. Schematic of computational model.	4
Figure 3. Computational model of original sabot.	5
Figure 4. Expanded view of sabot cup: original (left) and modified (right).	5
Figure 5. The 2-D structured mesh for original sabot.	6
Figure 6. Computational mesh for 3-D model with modified sabot.	7
Figure 7. Mach contours for 2-D ZNSFLOW.	9
Figure 8. Mach contours for 2-D CFD++.	9
Figure 9. Mach contours for 2-D FLUENT.	10
Figure 10. Pressure contours for 2-D ZNSFLOW.	10
Figure 11. Pressure contours for 2-D CFD++.	11
Figure 12. Pressure contours for 2-D FLUENT.	11
Figure 13. Comparison of C_p along centerline for 2-D cases.	12
Figure 14. Mach contours for 3-D ZNSFLOW.	13
Figure 15. Mach contours for 3-D CFD++.	13
Figure 16. Mach contours for 3-D FLUENT.	14
Figure 17. Pressure contours for 3-D ZNSFLOW.	14
Figure 18. Pressure contours for CFD++.	15
Figure 19. Pressure contours for 3-D FLUENT.	15
Figure 20. Surface pressure for 3-D CFD++.	16
Figure 21. Surface pressure for 3-D ZNSFLOW.	17
Figure 22. Surface pressure for 3-D FLUENT.	17
Figure 23. Comparison of C_p along the projectile centerline for 3-D cases.	18
Figure 24. Comparison of C_p along 60° plane for modified sabot.	18
Figure 25. Comparison of centerline C_p for original and modified sabot, CFD++ solutions.	19

List of Tables

Table 1. Dimensions for structured grids.....	6
Table 2. Elements for unstructured grids.....	7
Table 3. Axial forces.....	19

Acknowledgments

The authors would like to thank Harris Edge, U.S. Army Research Laboratory (ARL) Weapons and Analysis Branch, Aberdeen Proving Ground, MD, for his contributions to this work. As a former member of the computational fluid dynamics team, he provided the initial computational mesh for this study.

This work was supported by a grant of computer time from the Department of Defense High Performance Computing Major Shared Resource Center at ARL.

1. Introduction

The use of computational fluid dynamics (CFD) in the areas of projectile design and development is a continuously evolving field. Improved computer technology and state-of-the-art numerical procedures enable scientists to develop solutions to complex, three-dimensional (3-D) problems associated with projectile and missile systems of interest to the U.S. Army. Many geometrically complex single-body and multibody systems have been investigated using commercial as well as in-house CFD software packages (1–7). The focus of this study is a kinetic energy (KE) projectile with an experimental sabot design. The computational problem involves two-dimensional (2-D) and 3-D flow computations at a Mach number of 4.5 and at a 0° angle of attack for both the original and the modified sabots. The sabot petals separate from the projectile after the sabot leaves the gun barrel. So the results from this study are only valid for an instant at muzzle exit. The original purpose of the study was to get a quantitative estimate of the surface pressure values on the sabot at that instant. This report describes the application of several CFD solvers to this problem.

2. Flow Solvers

2.1 ZNSFLOW Code

The ZNSFLOW solver is a product of a common high performance computing software support initiative (CHSSI) project (8). It is a descendant of F3D, a code used successfully for many years on Cray vector processors such as the C90. The complete set of 3-D time-dependent, generalized-geometry, Reynolds-averaged, thin-layer Navier-Stokes equations is solved using the finite volume method in general spatial coordinates using an implicit, approximately factored scheme with an upwind scheme in the stream-wise direction and central differencing in the other two directions. The complete set of 3-D, time-dependent, generalized-geometry, Reynolds-averaged, thin-layer Navier-Stokes equations is solved numerically to obtain a solution to this problem and can be written in general spatial coordinates ξ , η , and ζ as follows:

$$\partial_\tau \hat{q} + \partial_\xi \hat{F} + \partial_\eta \hat{G} + \partial_\zeta \hat{H} = \text{Re}^{-1} \partial_\zeta \hat{S}, \quad (1)$$

where

- $\xi = \xi(x, y, z, t)$ —longitudinal coordinate,
- $\eta = \eta(x, y, z, t)$ —circumferential coordinate,

- $\zeta = \zeta(x, y, z, t)$ —nearly normal coordinate, and
- $\tau = t$ —time.

Under CHSSI, the code was rewritten to provide scalable performance on a number of computer architectures. Programming enhancements include the use of dynamic memory allocation and highly optimized cache management. ZNSFLOW features a graphical user interface to facilitate problem setup. The flow solver can be used for problems using structured zonal grids as well as Chimera overset grids for complex geometrical configurations. For turbulent flows, the algebraic eddy viscosity turbulence model developed by Baldwin and Lomax (9), a one-equation Rt model and a two-equation $k-\epsilon$ model are available. For the original sabot, the $k-\epsilon$ model was used, while the Baldwin-Lomax model was used for the modified sabot. (The reason for this will be discussed later.) Second-order spatial discretization was used in both cases.

2.2 CFD++ Code

CFD++ (10, 11) is a commercially available code that can be used for either steady-state or time-accurate unsteady CFD problems. The basic numerical framework of this code is one that implements a unified grid, unified physics, and unified-computing approach. The 3-D, time-dependent Reynolds-averaged Navier-Stokes (RANS) equations are solved using the finite volume method:

$$\frac{\partial}{\partial \tau} \int_V \mathbf{W} dV + \oint [\mathbf{F} - \mathbf{G}] \cdot d\mathbf{A} = \int_V \mathbf{H} dV, \quad (2)$$

where \mathbf{W} is the vector of conservative variables, \mathbf{F} and \mathbf{G} are the inviscid and viscous flux vectors, respectively, \mathbf{H} is the vector of source terms, V is the cell volume, and A is the surface area of the cell face. Second-order spatial discretization was used.

The numerical framework of CFD++ is based on the following general elements:

- unsteady compressible and incompressible Navier-Stokes equations with turbulence modeling (unified-physics),
- unification of Cartesian, structured curvilinear, and unstructured grids, including hybrids (unified-grid),
- unification of treatment of various cell shapes including hexahedral, tetrahedral, and triangular prism cells (3-D), quadrilateral and triangular cells (2-D), and linear elements (one-dimensional [1-D]) (unified-grid),
- treatment of multiblock patched aligned (nodally connected), patched-nonaligned and overset grids (unified-grid),
- total variation diminishing discretization based on a new multidimensional interpolation framework,

- Riemann solvers to provide proper signal propagation physics, including versions for preconditioned forms of the governing equations,
- consistent and accurate discretization of viscous terms using the same multidimensional polynomial framework,
- point-wise turbulence models that do not require knowledge of distance to walls,
- versatile boundary condition implementation that includes a rich variety of integrated boundary condition types for the various sets of equations, and
- implementation on massively parallel computers based on the distributed memory message passing model using native message-passing libraries or message passing interface, parallel virtual machine, etc. (unified-computing).

2.3 FLUENT Code

FLUENT (12) is another commercially available code that solves steady-state and time-accurate CFD problems on unstructured grids. The FLUENT software suite has several solvers for both incompressible and compressible flows in both an implicit and explicit numerical framework. The implicit, compressible (coupled) CFD solver was used for this study. The 3-D, time-dependent, RANS equations are solved using the finite volume method as defined in equation 2.

The inviscid flux vector \mathbf{F} is evaluated by a standard upwind flux-difference splitting. In the implicit solver, each equation in the coupled set of governing equations is linearized implicitly with respect to all dependent variables in the set, resulting in a block system of equations. A block Gauss-Seidel, point implicit linear equation solver is used with an algebraic multigrid method to solve the resultant block system of equations. The coupled set of governing equations is discretized in time and time marching proceeds until a steady state solution is reached. In the implicit scheme, which was used in this study, an Euler-implicit discretization in time is combined with a Newton-type linearization of the fluxes. Second-order spatial discretization was used.

Several turbulence models are available; the two-equation realized $k-\epsilon$ turbulence model was used for these calculations. Due to the complexity of the model geometry, the solution was started with first-order discretization. When the solution was stabilized, second-order discretization was used for the final solution.

3. Projectile and Model Geometry

3.1 Projectile System

The projectile of interest for this study is the M829A2. It is a long-rod KE round that is one of a family of weapons used with the M1 Abrams tank. Figure 1 is a drawing of the round, showing the projectile, sabot, and cartridge.

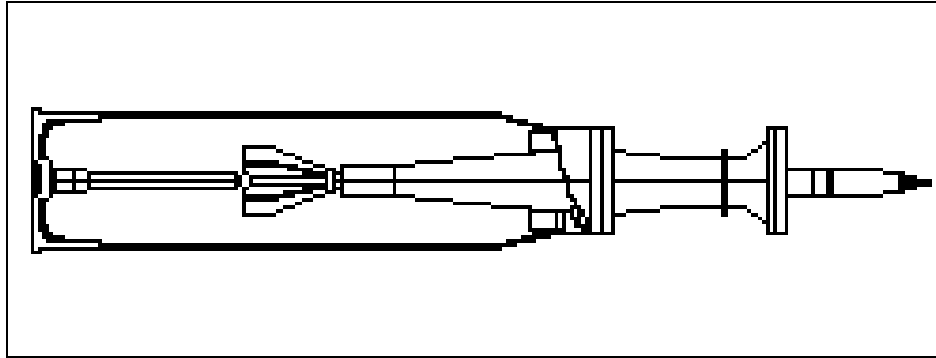


Figure 1. Drawing of an M829A2 round.

3.2 Computational Models

The computational model consists of a 635-mm-long projectile with sabot. The diameter of the projectile is ~24 mm. The sabot begins 75 mm from the tip of the projectile. For purposes of this study, the section of the projectile after the sabot (i.e., the tail fin) was not modeled. The schematic shown in Figure 2 depicts an outline of the model along the axis of symmetry. This configuration represents the projectile for an instant at muzzle exit, prior to the removal of the sabot petals via the aerodynamic forces.

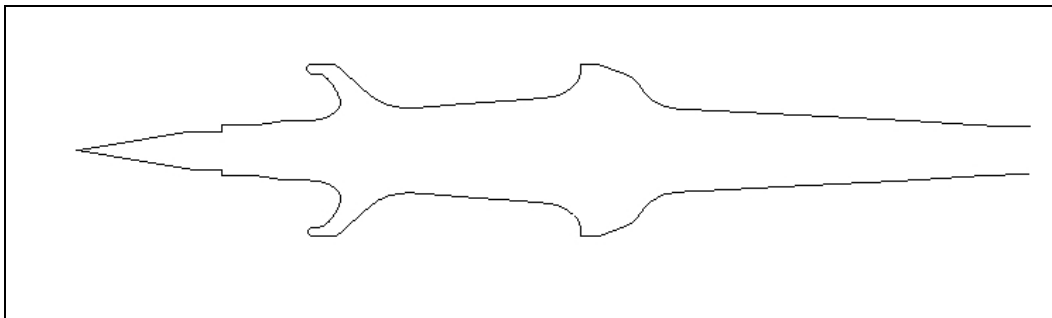


Figure 2. Schematic of computational model.

Two computational models were used, one for the original sabot design and one for the modified (experimental) sabot design. For the most part, the two models are quite similar; the one difference is that the experimental model has an insert in the front cup of the sabot. Figure 3 shows the overall model for the original design. An expanded view of the sabot cup for both the original and modified sabots is shown in Figure 4.

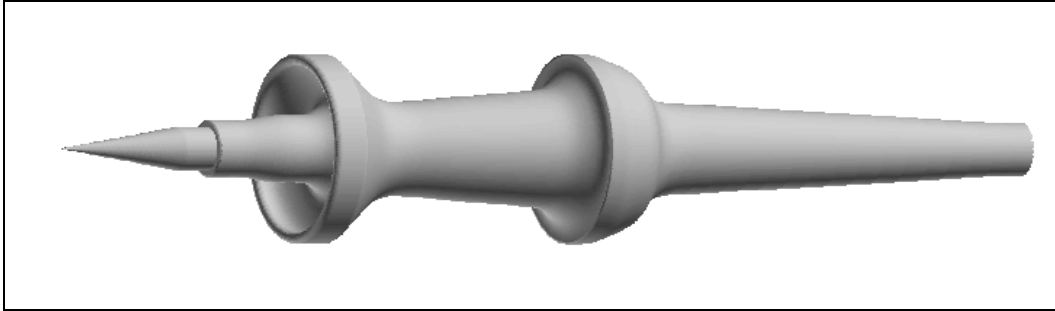


Figure 3. Computational model of original sabot.

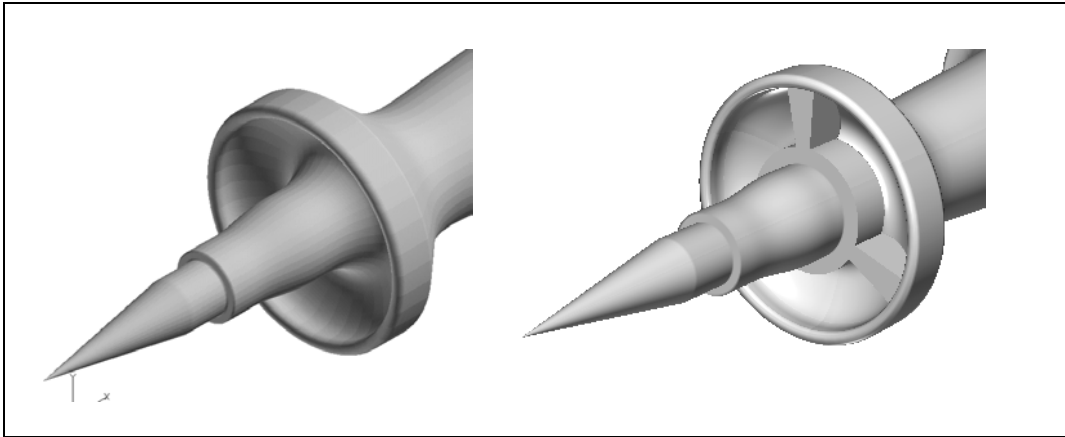


Figure 4. Expanded view of sabot cup: original (left) and modified (right).

4. Computational Meshes

4.1 ZNSFLOW Grids

For the ZNSFLOW cases, two structured zonal grids were created. Because of the symmetry of the original sabot, a 2-D mesh was suitable for the computation of the flow field. For the experimental sabot, a 3-D mesh was required. In both cases, one large grid provides the mesh around the projectile and the original sabot. For the experimental model, a single smaller grid provides the mesh for the insert in the front cup of the sabot. Table 1 shows the specific details for each of these configurations.

Table 1. Dimensions for structured grids.

	Original Sabot	Modified Sabot	Sabot Insert
Longitudinal	188	222	30
Circumferential	3	36	25
Radial	59	59	21
Total points	33,276	471,528	15,750

The computational meshes were created using the various tools found in the OVERGRID Grid Generation software package (13). Figure 5 shows a single-plane 2-D mesh for the original sabot. The boundary conditions consist of a collapsed axis at the nose of the projectile, supersonic outflow at the rear of the mesh, no-slip wall conditions on the projectile surface, and far field (pressure- and temperature-based inflow/outflow) at the outer edge.

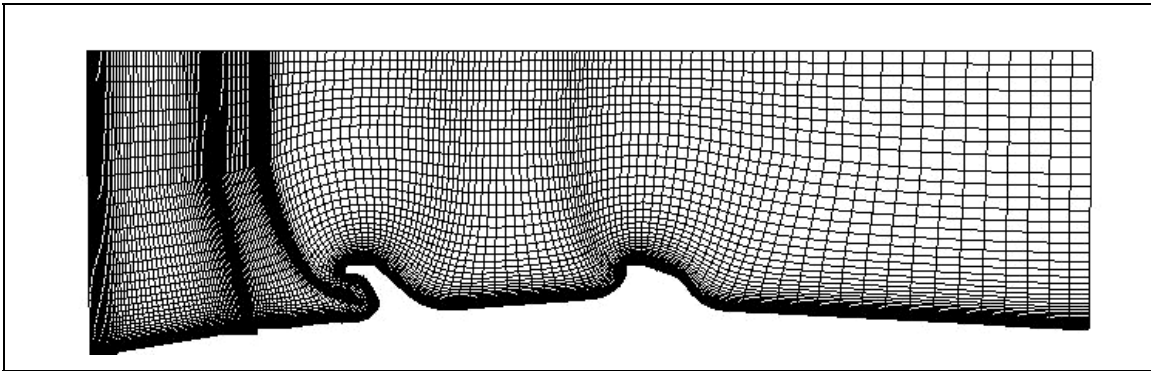


Figure 5. The 2-D structured mesh for original sabot.

Figure 6 shows a cross-sectional view of the 3-D mesh for the modified sabot configuration. Note that due to the periodicity of the modified design, it was only necessary to model a 60° wedge for the computation. In addition to the boundary conditions for the 2-D case, symmetry plane conditions for the circumferential boundaries and isothermal wall conditions for the surfaces of the sabot insert were included in the parameters of the solution.

4.2 CFD++ Grids

Using the grid tools available in the CFD++ software package, the structured grids created for the ZNSFLOW cases were converted into unstructured grids for compatibility with the CFD++ solver. Physically, the mesh retained its hexagonal cell structure. Logically, it is now referenced by cells, nodes, and faces instead of longitudinal, circumferential, and normal gridpoint indices. Any zonal boundaries are merged so that the resulting mesh is one large entity. External boundary conditions remain as before. Table 2 shows the size of the unstructured grids for both the original 2-D and modified 3-D sabot designs.

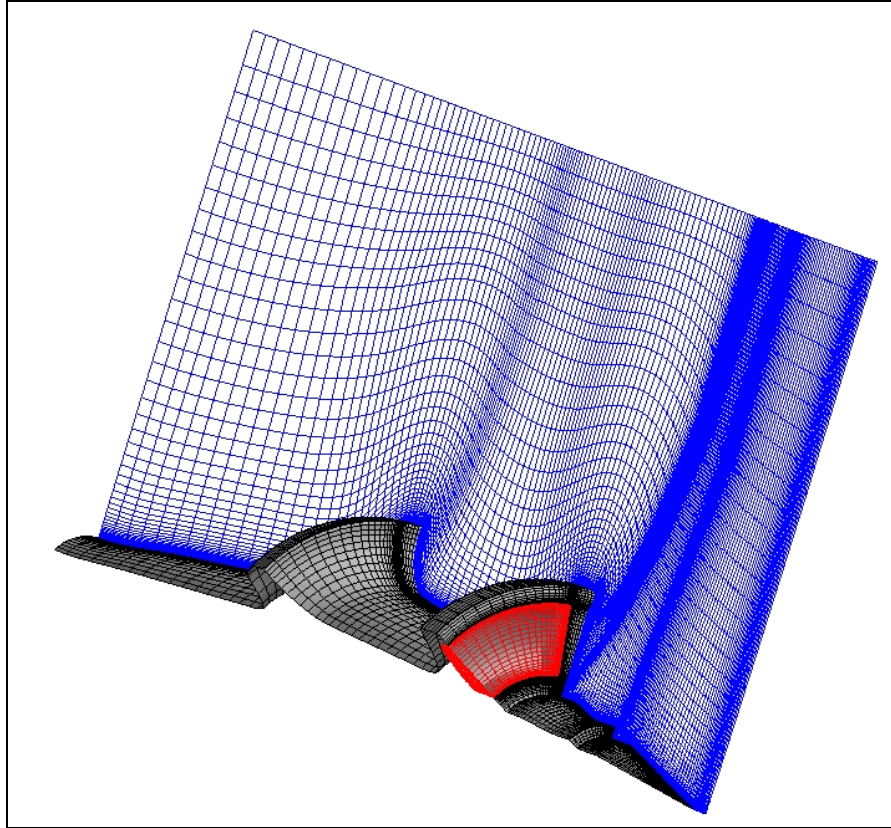


Figure 6. Computational mesh for 3-D model with modified sabot.

Table 2. Elements for unstructured grids.

	Original Sabot	Modified Sabot
Cells	10,730	461,854
Nodes	10,974	485,778
Faces	21,703	471,800

4.3 FLUENT Grids

As with the CFD++ solver, FLUENT requires the computational mesh to be unstructured. However, it must also be in a FLUENT specific format, as there are no conversion tools available in the software package. GRIDGEN (14) is a grid generation software package that has the capability of reading and writing various file formats, including PLOT3-D and FLUENT. It was used to convert the 2-D grid. However, due to a bug in the GRIDGEN code, it could not correctly output the collapsed axis boundary in the 3-D grid to a FLUENT mesh file. The mesh had to be slightly modified by patching the grid at the nose of the projectile. This eliminated the need for a boundary condition specification along the symmetry axis in front of the projectile. The model geometry was not changed, and the remainder of the grid retained its original structure. The size of the grid only changed by 3366 cells (or <1%).

5. Results

Several computations were performed using the three flow solvers and the two different sabot models described previously. Study parameters include Mach number of 4.5, 0° angle of attack, and standard atmospheric flight conditions. For each solver, boundary conditions (as described in the previous section) were selected to provide as reasonable a comparison as possible, given the choices and constraints of each code. A modified two-equation k - ϵ turbulence model was selected in each case. However, after over 100,000 iterations, the ZNSFLOW (3-D) modified sabot case was not converged; the Baldwin-Lomax model was used instead for the final solution. Initially, the free-stream was set to zero near the wall boundary for CFD++ and FLUENT; this option is not available in ZNSFLOW. All computations were performed on the SGI suite computers at the ARL Major Shared Resource Center (MSRC). Resources required for the 2-D computations were minimal. For the 3-D calculations, resources used differed depending on the solver used, but were also minimal.

Each of the CFD software packages used in this study has internal graphical capabilities for viewing the flow field solution while the computation is in progress. Additionally, the files can be reformatted and used with other available postprocessors. For all cases in this study, the grid and solution files were reformatted and then imported into FIELDVIEW (15), a scientific visualization software package.

5.1 Original Sabot

Contour plots in the symmetry plane are used to compare the 2-D solutions for the original sabot. Figures 7 and 8 show the Mach contours to be quite similar, though the shock waves off the sabot cup are more defined in the CFD++ solution (Figure 8). Figure 9 shows the same characteristics, with slightly more definition of the flow field in front of the sabot cup. Similarly, all three pressure contours (Figures 10–12) show similar flow characteristics. The area of high pressure in front of the sabot cup and the shock wave at the edge of the cup are visible in all three flow fields. The FLUENT solution (Figure 12) shows a more defined area of low pressure in front of the sabot cup.

A comparison of the pressure coefficient (C_p) along the centerline of the projectile, Figure 13, shows the solutions to be qualitatively similar. The differences in the curves directly correspond to some of the differences in the flow field in the previous figures. The increase in C_p at ~ 0.06 m coincides with the oblique shock wave formed at the end of the conical nose of the projectile. This shock wave forms a small distance forward of the conical-cylindrical intersection in the FLUENT case (Figures 9 and 12), while in the other cases it forms closer to the intersection. Both ZNSFLOW and CFD++ show a sharp increase at ~ 0.1 m, where the flat face of the sabot petal begins, while FLUENT shows a very small increase. CFD++ shows the largest increase

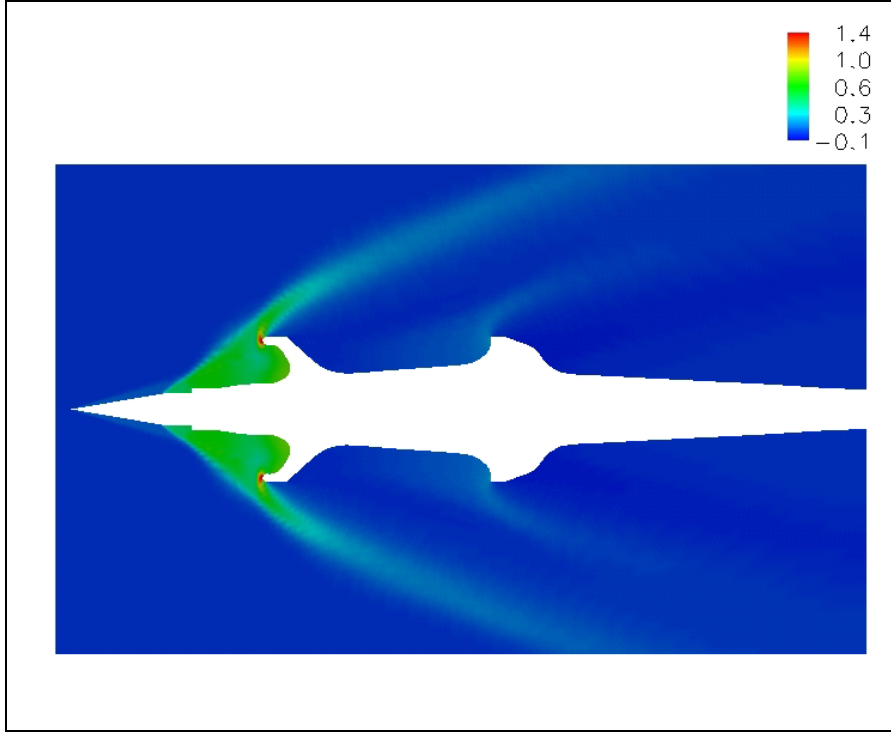


Figure 7. Mach contours for 2-D ZNSFLOW.

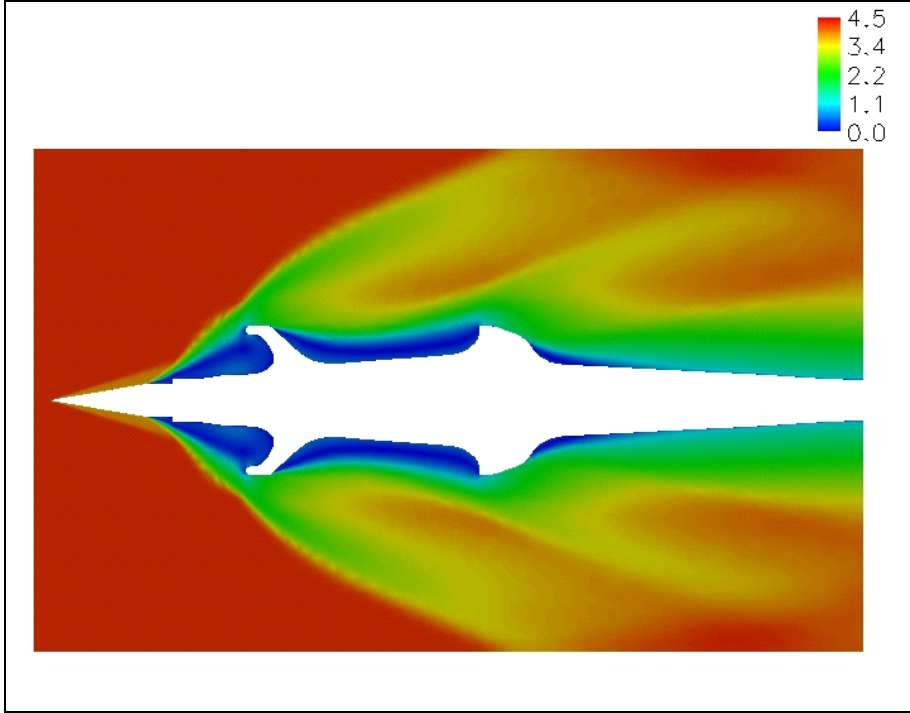


Figure 8. Mach contours for 2-D CFD++.

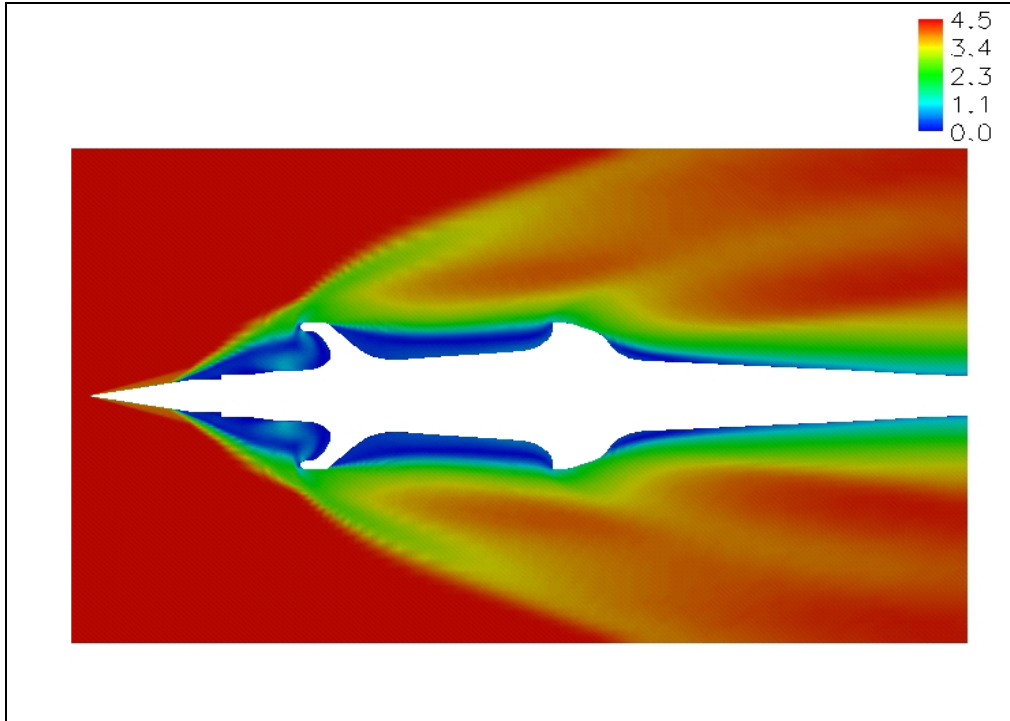


Figure 9. Mach contours for 2-D FLUENT.

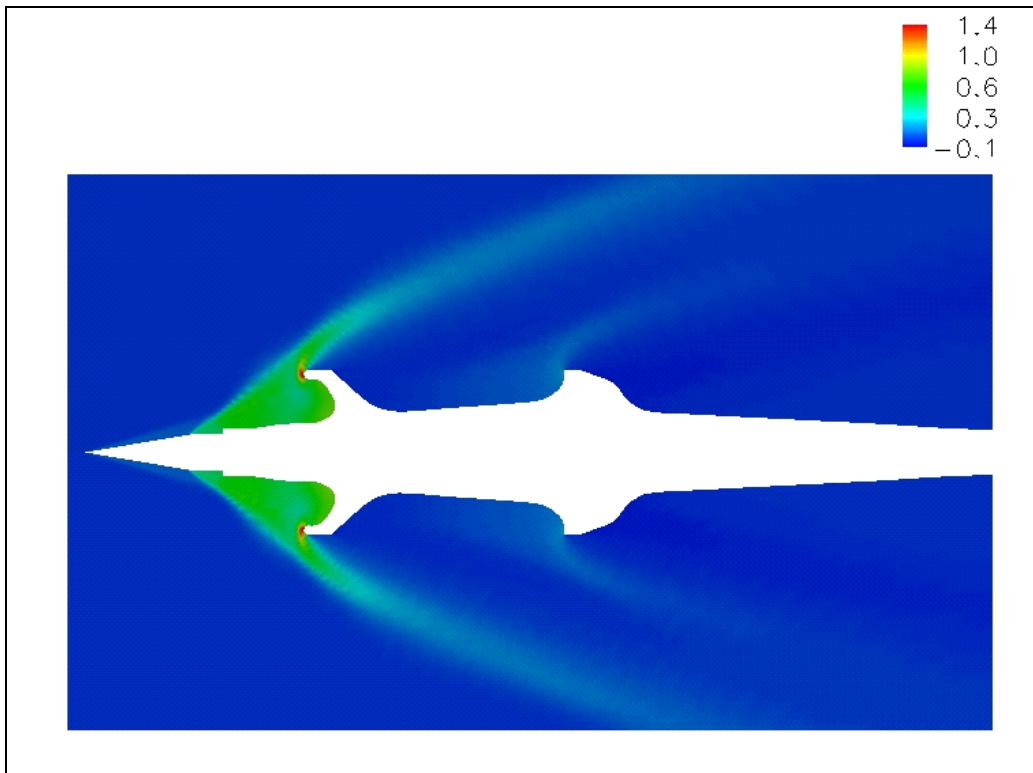


Figure 10. Pressure contours for 2-D ZNSFLOW.

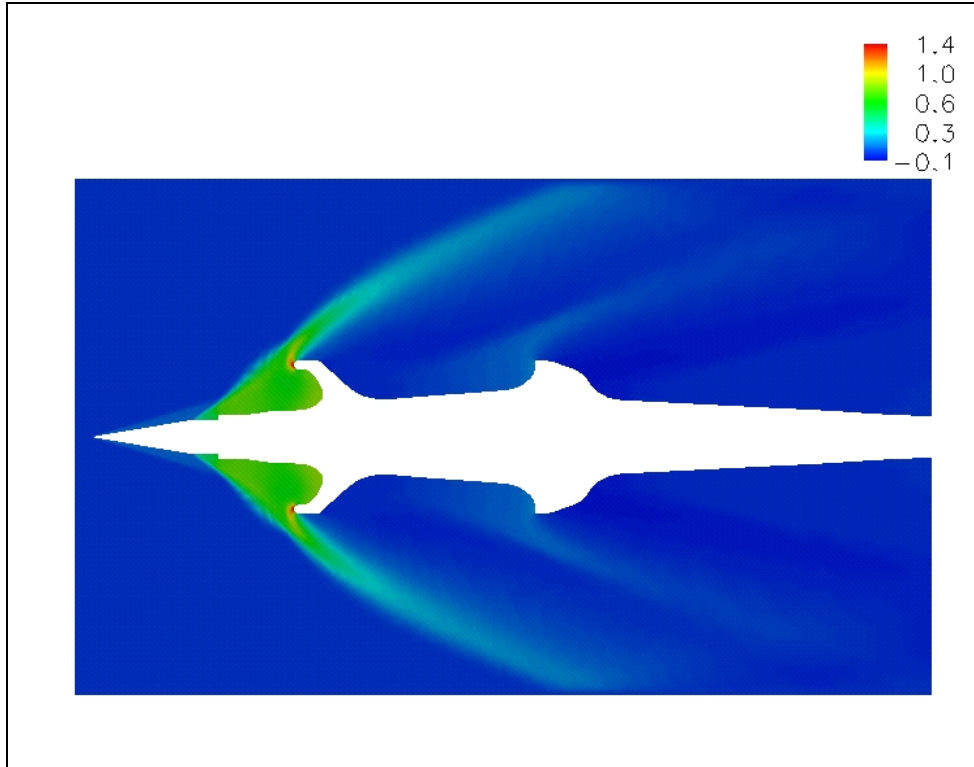


Figure 11. Pressure contours for 2-D CFD++.

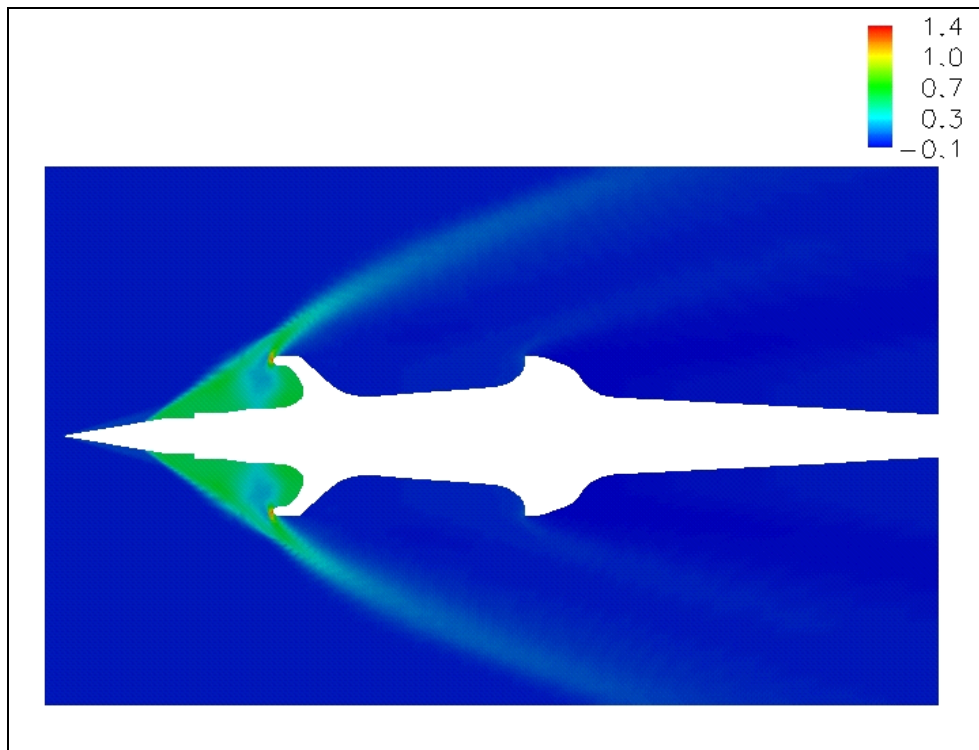


Figure 12. Pressure contours for 2-D FLUENT.

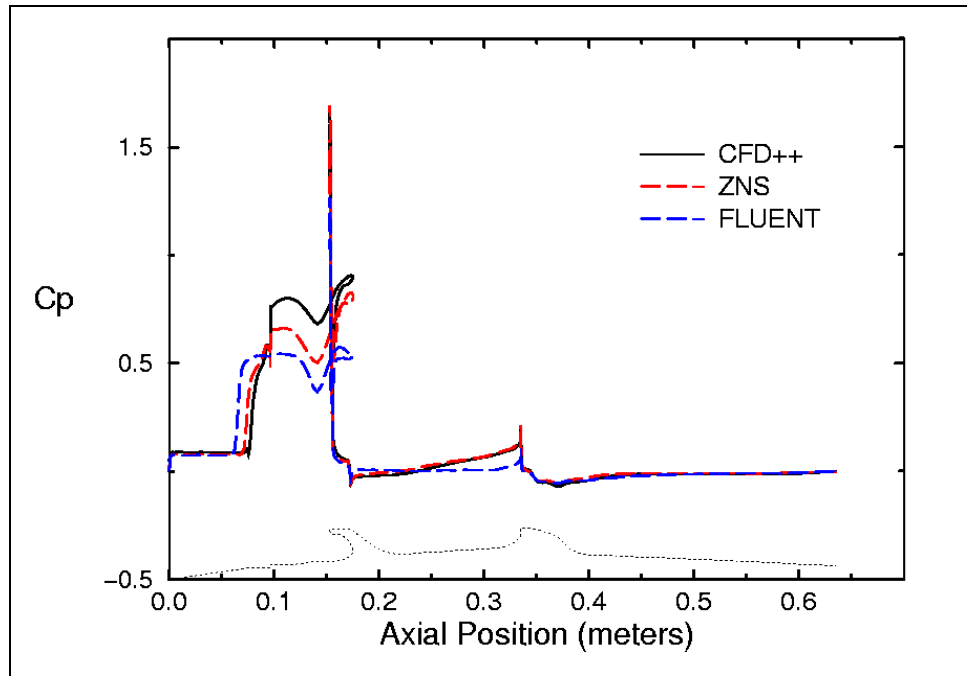


Figure 13. Comparison of C_p along centerline for 2-D cases.

in pressure, 21% higher than the ZNSFLOW solution at ~ 0.11 m, while the FLUENT solution gives the lowest peak pressure, 18% lower than the ZNSFLOW solution. All three solutions show a qualitatively similar reduction in pressure as the flow expands past the first conical-cylindrical section of the sabot at ~ 0.14 m. The largest expansion was in the FLUENT solution, which gave a minimum pressure 31% lower than the (first) maximum. The reduction in pressure was 24% and 15% in the ZNSFLOW and CFD++ solutions, respectively. This expansion is more evident in the flow field plots for the FLUENT case (Figures 9 and 12) due to the plotting scales, but it is present in all cases. The pressure in the sabot cup is qualitatively similar in all three cases. The CFD++ and ZNSFLOW solutions show a large reduction in pressure and a monotonically increasing pressure between the cup and the obturator, while the FLUENT solution shows a low, constant pressure.

5.2 Modified Sabot

Multiplane contour plots are used to represent the 3-D solutions for the modified (experimental) sabot. The Mach contours shown in Figures 14–16 show the solutions to be similar. However, the contours in Figures 15 and 16 (CFD++ and FLUENT, respectively) are more clearly defined, especially along the nose of the projectile. Figures 17–19 show pressure contours in the symmetry planes of the flow fields. All three solutions show the shock at the edge of the sabot cup, but the contours for the ZNSFLOW solution (Figure 17) are much less defined. The final three figures show the surface pressure on the projectile model for each of the calculations. The

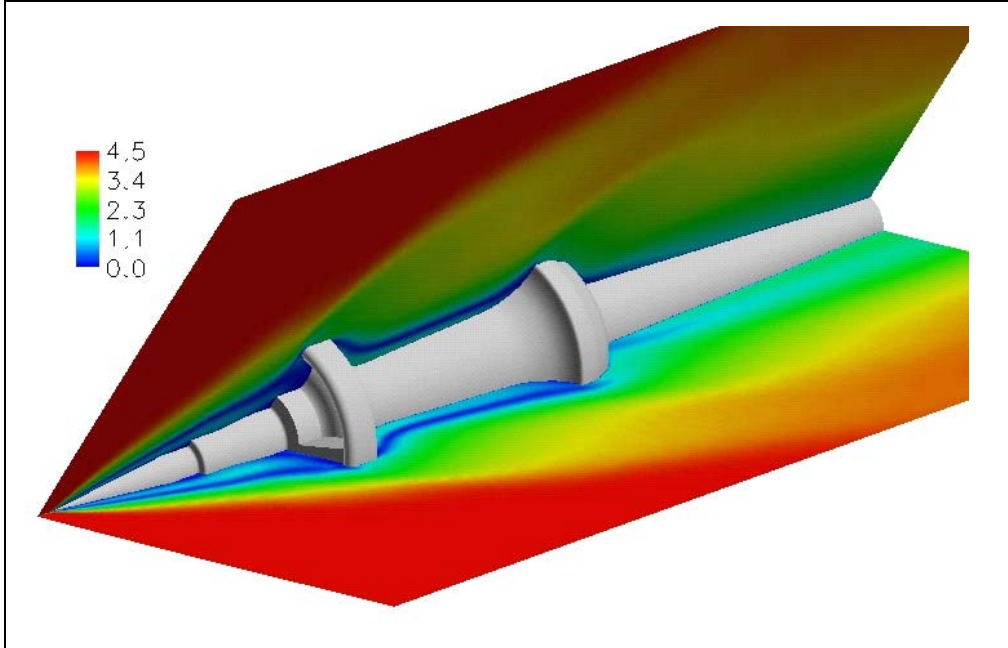


Figure 14. Mach contours for 3-D ZNSFLOW.

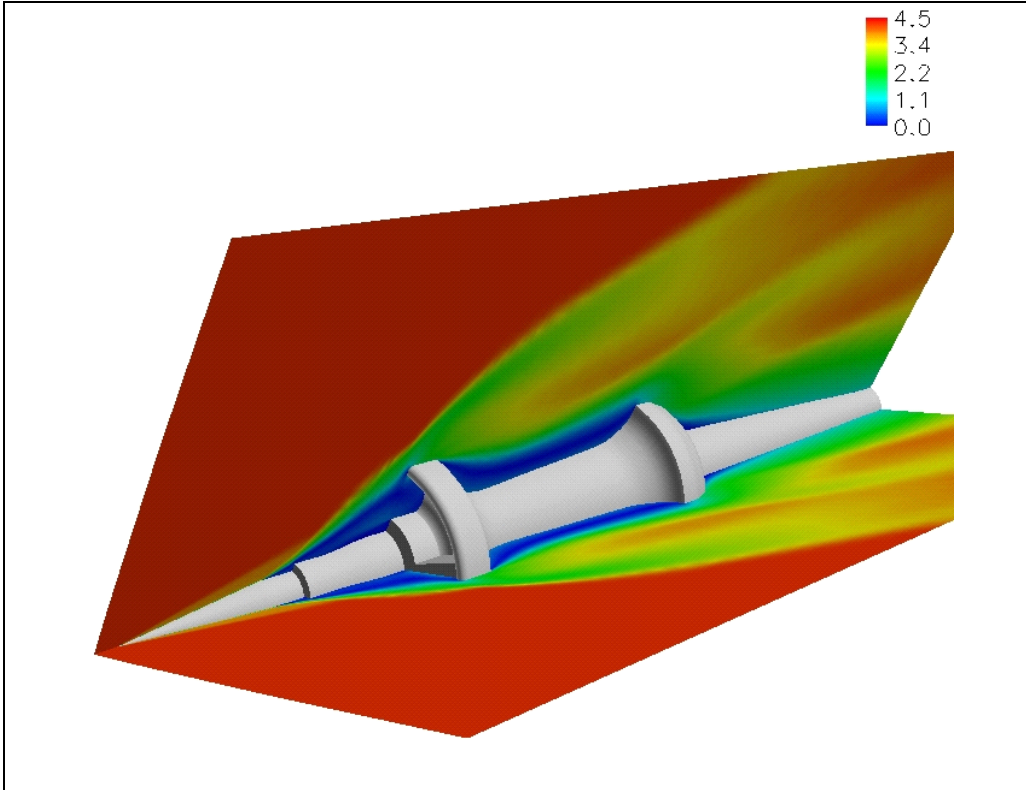


Figure 15. Mach contours for 3-D CFD++.

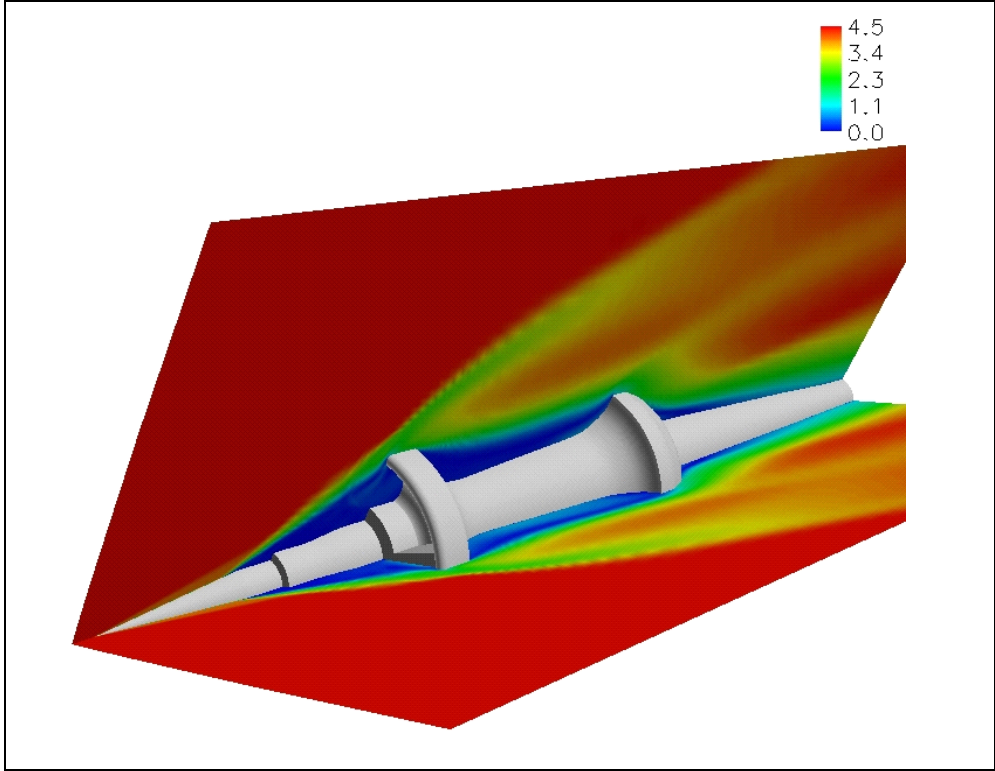


Figure 16. Mach contours for 3-D FLUENT.

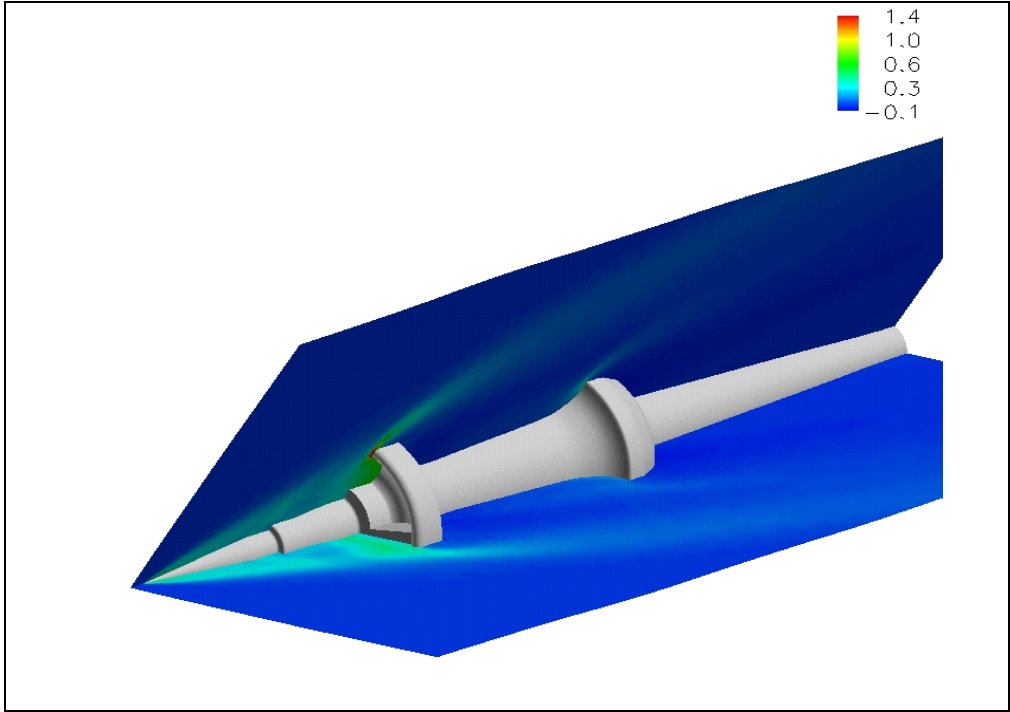


Figure 17. Pressure contours for 3-D ZNSFLOW.

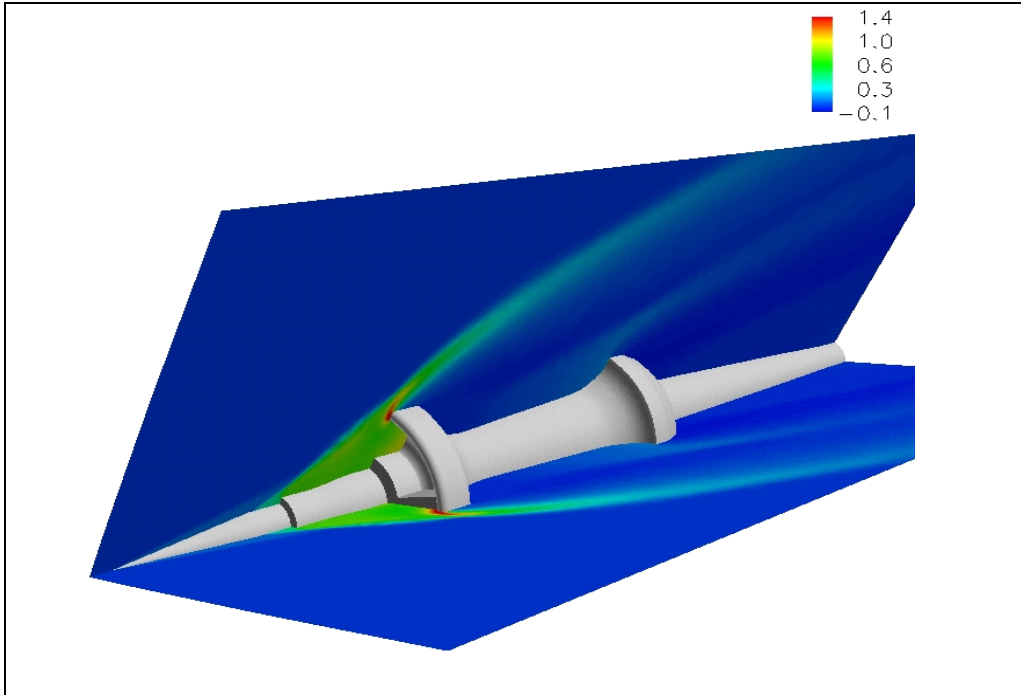


Figure 18. Pressure contours for CFD++.

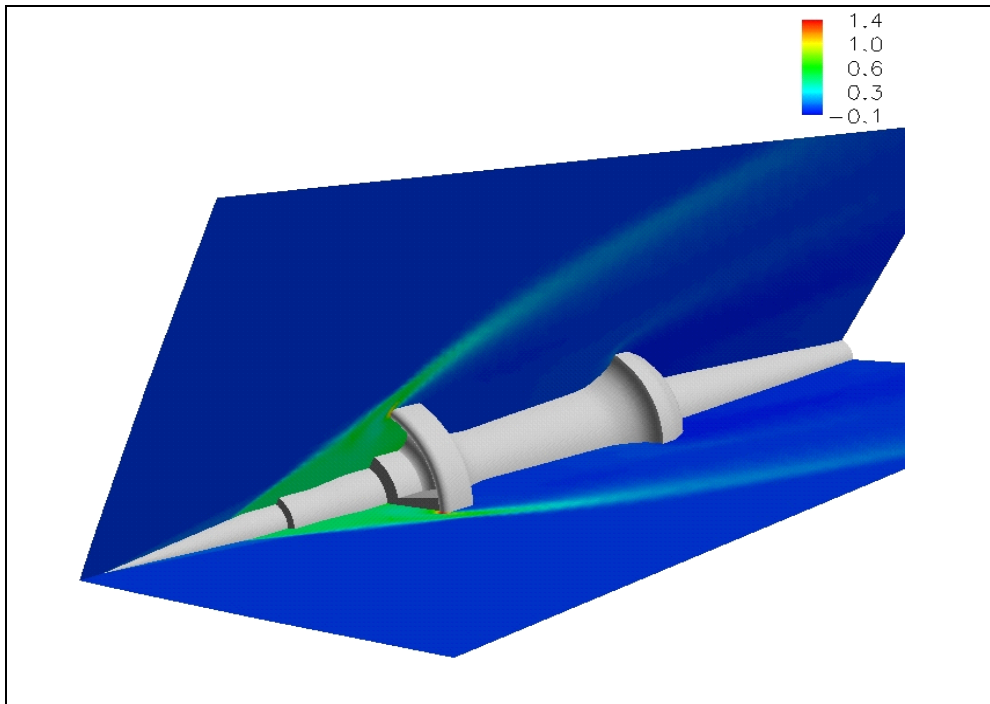


Figure 19. Pressure contours for 3-D FLUENT.

pressure on the edge of the front cup is more prominent in Figure 20 (FLUENT) than in Figures 21 and 22. All three figures, however, show the same overall qualities of higher pressure in front of the cup and lower pressure along the rest of the sabot.

As seen previously in the original sabot, the C_p values along the centerline of the projectile (Figure 23) are quite similar for the CFD++ and FLUENT solutions. For the ZNSFLOW results, there is quite a difference in the values in front of the sabot cup; the pressure is slightly higher at the obturator as well. This is most likely due to the fact that a converged solution could not be achieved for this case with the two-equation turbulence model. Similar trends appear along the 60° plane. As seen in Figure 24, all three solutions are similar, except in the area in front of the insert. Figure 25 shows a comparison of the C_p values for the original and modified sabots, using the CFD++ solver. The pressure on the modified sabot is slightly higher in the area in front of the sabot cup (near 0.14 m) and ~20% higher in the cup itself, in the area between 0.14 m and 0.17 m. Otherwise, the two sabot models show nearly identical values.

5.3 Force Comparison

In addition to the qualitative comparisons of the flow fields, it is useful to compare some quantitative variables. For ZNSFLOW, these variables must be extracted in the post-processing procedure; CFD++ and FLUENT provide the option to have them calculated as the solution progresses. Table 3 shows the axial force in Newtons for a 60° wedge of the actual projectile. For the original sabot, the forces from all three solvers are only slightly different. For the modified sabot cases, using the ZNSFLOW solution as the mean, FLUENT and CFD++ are ~10% lower and higher, respectively. The difference in the axial force follows directly from differences in the predicted maximum pressures (Figure 13).

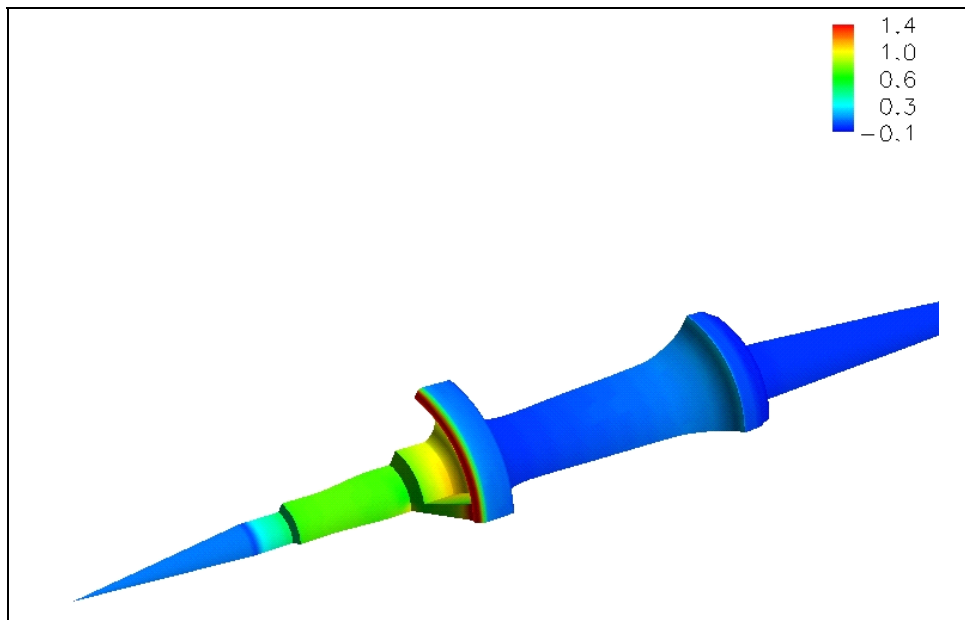


Figure 20. Surface pressure for 3-D CFD++.

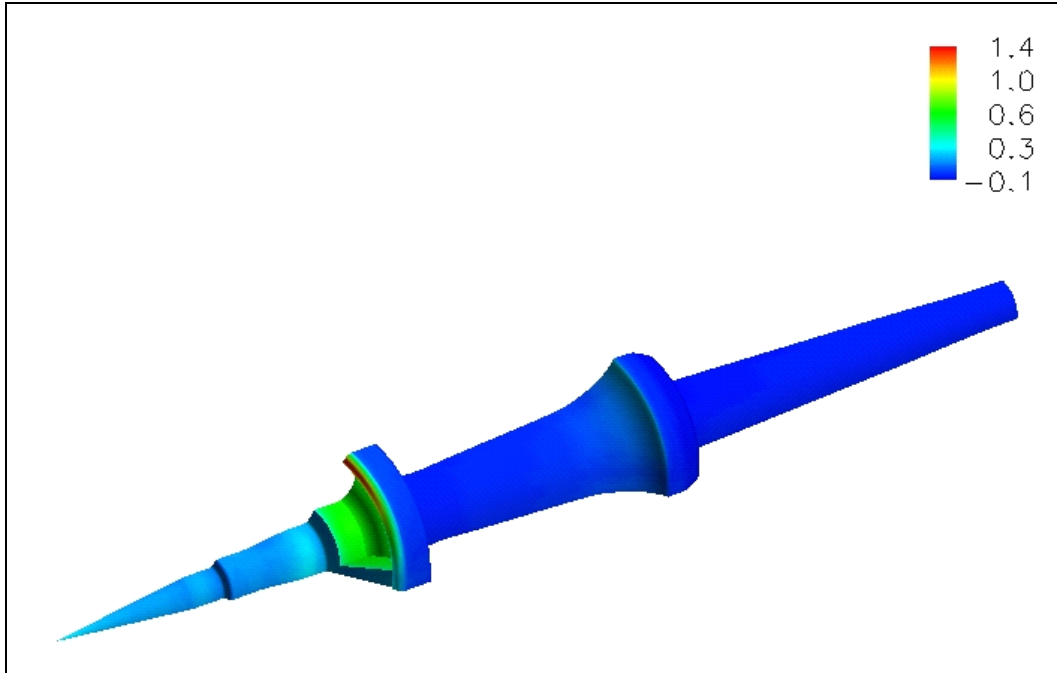


Figure 21. Surface pressure for 3-D ZNSFLOW.

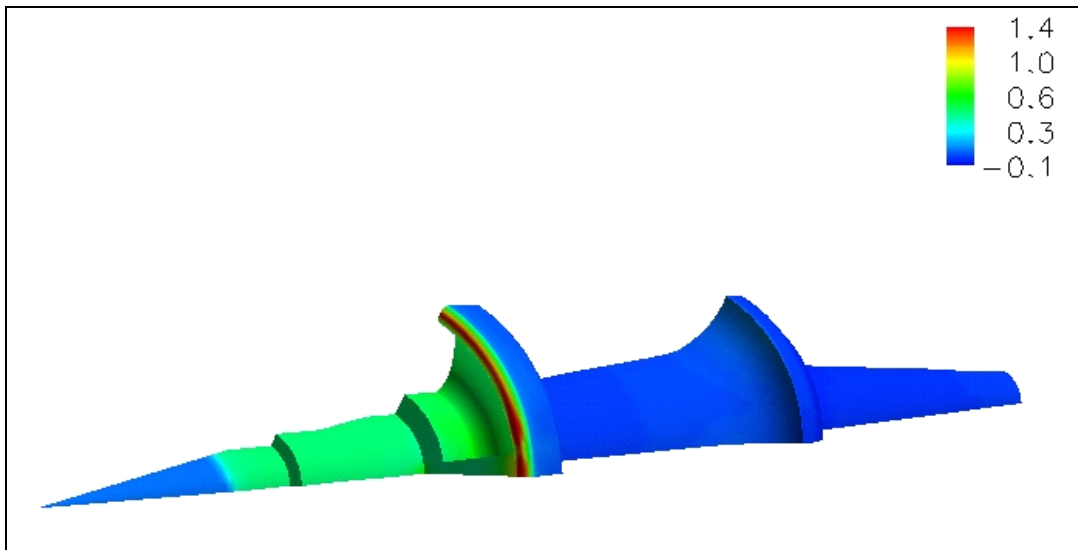


Figure 22. Surface pressure for 3-D FLUENT.

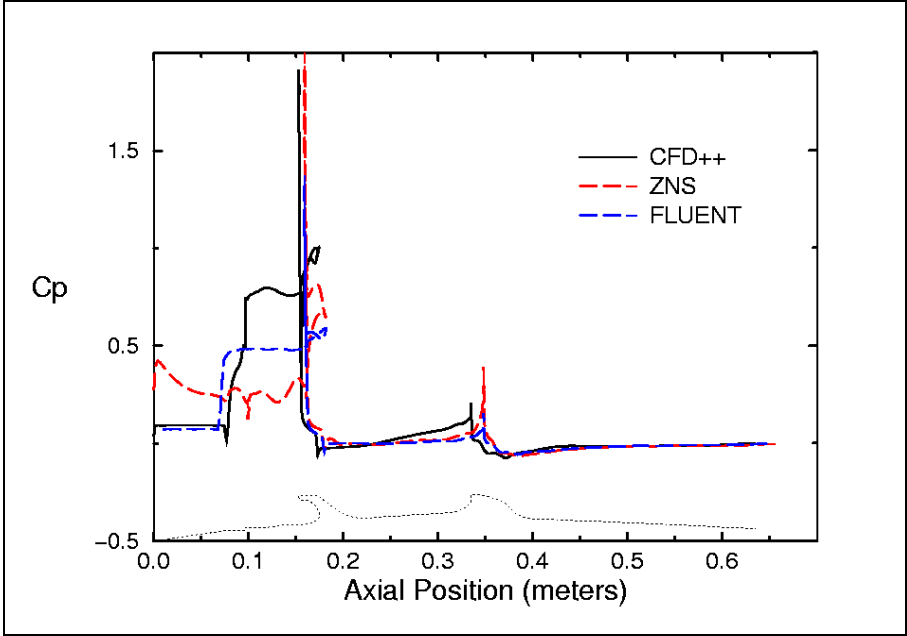


Figure 23. Comparison of C_p along the projectile centerline for 3-D cases.

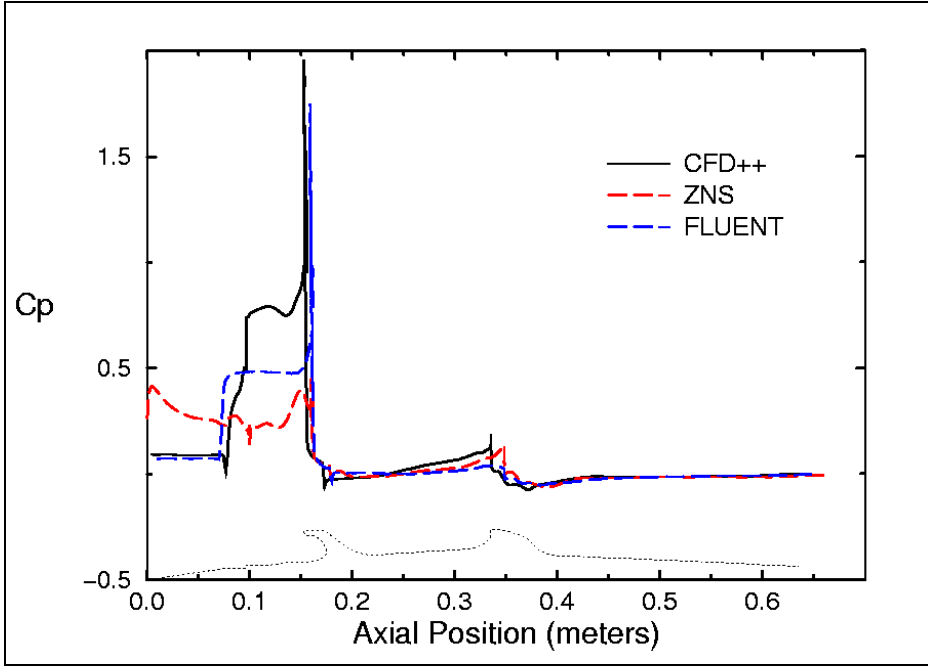


Figure 24. Comparison of C_p along 60° plane for modified sabot.

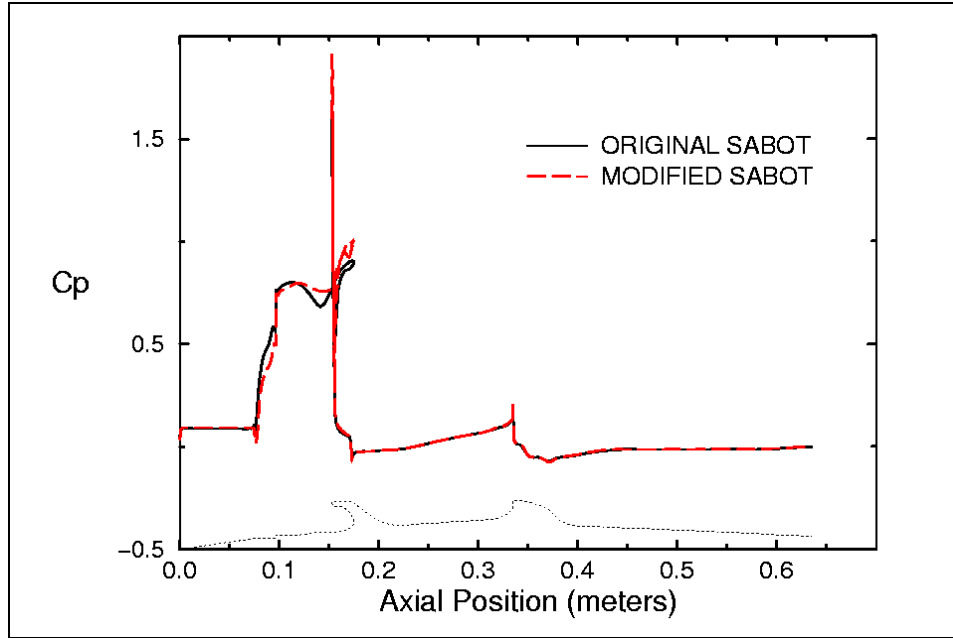


Figure 25. Comparison of centerline Cp for original and modified sabot, CFD++ solutions.

Table 3. Axial forces.

	Original Sabot	Modified Sabot
FLUENT	1777 N	1863 N
ZNSFLOW	1722 N	2011 N
CFD++	1799 N	2161 N

5.4 Solver Differences

This model problem is a fairly difficult test case and all three solvers performed reasonably. It is difficult to quantify for this case which solver gave the most accurate results because there is no test data available for validation. In fact, the primary purpose of the study was to get an estimate of the surface pressure on the sabot petals because they cannot be experimentally determined.

A statement on the performance of the solvers in getting the final answers can be made. Although the details provided are specific to the 3-D solutions, the comments in general also apply to the 2-D cases.

CFD++ was the most robust and obtained a final solution in the least time and least number of iterations. It took ~2000 iterations to converge the axial force to a constant value, and the residuals dropped about three orders of magnitude.

ZNSFLOW took over 20,000 iterations to achieve a converged solution, with many iterations used to get the solution “started” with smaller Courant (CFL) numbers and added dissipation. The Courant number and smoothing factors are increased manually until the residuals stabilize.

FLUENT took ~24,000 iterations, primarily because a first-order spatial discretization was run first, followed by the second-order case. The case was hard to start from the second-order solution directly. Also, the CFL number was only increased to one. The residuals dropped from two orders of magnitude (the cross flow velocities) to four orders of magnitude (the turbulent KE and diffusivity).

Advantages of the CFD++ solver are its automatic CFL number ramping and a capability for adding dissipation parameters in the governing equations. In FLUENT, one must ramp the CFL number manually and there are no added dissipation parameters in the governing equations. This difficult test case is the first in which FLUENT has been difficult to run at higher CFL numbers. In previous cases (1, 2), simulations were started with the second-order spatial discretization solver, at CFL numbers of 1 or 2, and with a maximum CFL number between 5 and 10.

6. Conclusion

A computational study was undertaken to investigate the application of several CFD solvers to a computational model of a projectile system with two different sabots. Flow field computations were performed at Mach number 4.5 for 0° angle of attack, under standard atmospheric conditions. The computational results show the predictive capabilities of various CFD techniques in the analysis of supersonic flow for both a 2-D axisymmetric model and a 3-D model. They also provide a look at some of the software tools available to research scientists in the field of CFD. All three solvers provided qualitatively similar results. CFD++ provided the solution in the most efficient manner.

7. References

1. Sahu, J.; DeSpirito, J.; Edge, H.; Sifton, S.; Heavey, K. Recent Applications of Structured and Unstructured Grid Techniques to Complex Projectile and Missile Configurations. *Proceedings of the 8th International Grid Generation and Computational Field Simulations*, Honolulu, HI, June 2002.
2. DeSpirito, J.; Vaughn, Jr., M. E.; Washington, W. D. *Numerical Investigation of Canard-Controlled Missile Using Planar and Grid Tail Fins, Part I: Supersonic Flow*; ARL-TR-2848; U.S. Army Research Laboratory: Aberdeen Proving Ground, MD, 2002.
3. Sahu, J.; Heavey, K. R.; Edge, H. L. *Numerical Computations of Supersonic Flow Over Elliptical Projectiles*; ARL-TR-2589; U.S. Army Research Laboratory: Aberdeen Proving Ground, MD, 2001.
4. Sahu, J.; Heavey, K. R. *Computational Fluid Dynamics Modeling of a 40-mm Grenade With and Without Jet Flow*; ARL-TR-2572; U.S. Army Research Laboratory: Aberdeen Proving Ground, MD, 2001.
5. Graham, M. J.; Weinacht, P.; Brandeis, J.; Angelini, R. *A Numerical Investigation of Supersonic Jet Interaction for Finned Bodies*; ARL-TR-2312; U.S. Army Research Laboratory: Aberdeen Proving Ground, MD, 2000.
6. Sahu, J.; Heavey, K. R.; Pressel, D.; Dinavahi, S. *Parallel Numerical Computations of Projectile Flow Fields*; ARL-TR-2019; U.S. Army Research Laboratory: Aberdeen Proving Ground, MD, 1999.
7. Sahu, J.; Edge, H. L.; Heavey, K. R.; Ferry, E. N. *Computational Fluid Dynamics Modeling of Multi-body Missile Aerodynamic Interference*; ARL-TR-1765; U.S. Army Research Laboratory: Aberdeen Proving Ground, MD, 1998.
8. Edge, H. L.; Sahu, J.; Sturek, W. B.; Pressel, D. M.; Heavey, K. R.; Weinacht, P.; Zoltani, C. K.; Nietubicz, C. J.; Clarke, J.; Behr, M.; Collins, P. *Common High Performance Computing Software Support Initiative (CHSSI) Computational Fluid Dynamics CFD-6 Project Final Report: ARL Block-Structured Gridding Zonal Navier-Stokes Flow (ZNSFLOW) Solver Software*; ARL-TR-2084; U.S. Army Research Laboratory: Aberdeen Proving Ground, MD, 2000.
9. Baldwin, B. L.; Lomax, H. *Thin Layer Approximation and Algebraic Model for Separated Turbulent Flows*; AIAA 78-257; American Institute of Aeronautics and Astronautics, Reston, VA, 1978.

10. Goldberg, U. C.; Peroomian, O.; Chakravarthy, S. A Wall-Distance Free K-E Model With Enhanced Near-Wall Treatment. *American Society of Mechanical Engineers Journal of Fluids Engineering* **1998**, *120*, 457–462.
11. *CFD++ User Manual, version 2.6.5*; Metacomp Technologies, Argoura Hills, CA.
12. *FLUENT 5.0 User's Guide, volume 2*; Fluent, Inc., Lebanon, NH, 1998.
13. Chan, W. M. *OVERGRID Software Documentation*. U.S. Army Research Laboratory-Major Shared Resource Center: Aberdeen Proving Ground, MD, April 1999.
14. *GRIDGEN, version 14.3 user's manual*; Pointwise Inc., Fort Worth, TX, 2002.
15. *FIELDVIEW, version 8 user's manual*; Intelligent Light, Lindhurst, NJ, 2001.

<u>NO. OF COPIES</u>	<u>ORGANIZATION</u>
2	DEFENSE TECHNICAL INFORMATION CENTER DTIC OCA 8725 JOHN J KINGMAN RD STE 0944 FT BELVOIR VA 22060-6218
1	COMMANDING GENERAL US ARMY MATERIEL CMD AMCRDA TF 5001 EISENHOWER AVE ALEXANDRIA VA 22333-0001
1	INST FOR ADVNCD TCHNLGY THE UNIV OF TEXAS AT AUSTIN 3925 W BRAKER LN STE 400 AUSTIN TX 78759-5316
1	US MILITARY ACADEMY MATH SCI CTR EXCELLENCE MADN MATH THAYER HALL WEST POINT NY 10996-1786
1	DIRECTOR US ARMY RESEARCH LAB AMSRL D DR D SMITH 2800 POWDER MILL RD ADELPHI MD 20783-1197
1	DIRECTOR US ARMY RESEARCH LAB AMSRL CS IS R 2800 POWDER MILL RD ADELPHI MD 20783-1197
3	DIRECTOR US ARMY RESEARCH LAB AMSRL CI OK TL 2800 POWDER MILL RD ADELPHI MD 20783-1197
3	DIRECTOR US ARMY RESEARCH LAB AMSRL CS IS T 2800 POWDER MILL RD ADELPHI MD 20783-1197

<u>NO. OF COPIES</u>	<u>ORGANIZATION</u>
	<u>ABERDEEN PROVING GROUND</u>
2	DIR USARL AMSRL CI LP (BLDG 305) AMSRL CI OK TP (BLDG 4600)

<u>NO. OF COPIES</u>	<u>ORGANIZATION</u>	<u>NO. OF COPIES</u>	<u>ORGANIZATION</u>
1	COMMANDER NAVAL SURFACE WARFARE CTR ATTN CODE B40 W YANTA DAHLGREN VA 22448-5100	1	COMMANDER US ARMY TACOM ARDEC BLDG 162S AMCPM DS MO P J BURKE PICATINNY ARSENAL NJ 07806-5000
1	COMMANDER NAVAL SURFACE WARFARE CTR CODE 420 A WARDLAW INDIAN HEAD MD 20640-5035	1	METACOMP TECHNOLOGIES INC S R CHAKRAVARTHY 28632-B ROADSIDE DRIVE SUITE 255 AGOURA HILLS CA 91301
1	AIR FORCE ARMAMENT LAB AFATL/FXA D BELK EGLIN AFB FL 32542-5434	2	FLUENT INC 10 CAVENDISH COURT CENTERRA RESOURCE PARK G STUCKERT T SCHEIDEGGER LEBANON NH 03766-1442
3	COMMANDER US ARMY TACOM ARDEC AMSTA AR FSF T BLDG 382 H HUDGINS J GRAU W KOENIG PICATINNY ARSENAL NJ 07806-5000		
			<u>ABERDEEN PROVING GROUND</u>
1	COMMANDER US ARMY TACOM AMSTA AR CCH B P VALENTI BLDG 65-S PICATINNY ARSENAL NJ 07806-5001	1	DIR USARL AMSRL WM J SMITH BLDG 4600 APG MD 21005-5069
1	COMMANDER US ARMY ARDEC SFAE FAS SD M DEVINE PICATINNY ARSENAL NJ 07806-5001	18	DIR USARL AMSRL CI HC R NOAIC AMSRL SL BE A MIKHAIL AMSRL WM B A W HORST JR AMSRL WM BA D LYON AMSRL WM BC P PLOSTINS J DESPIRITO B GUIDOS K HEAVEY (5 CPS) J NEWILL J SAHU S SILTON P WEINACHT WM BD B FORCH WM BF S WILKERSON
1	NAVAL AIR WARFARE CENTER MS 3 BLDG 2187 D FINDLAY PATUXENT RIVER MD 20670		
1	UNIV OF ILLINOIS AT URBANA CHAMPAIGN DEPT OF MECHANICAL AND INDUSTRIAL ENGINEERING J C DUTTON URBANA IL 61801		